Two-fluid equilibrium with flow: FLOW2

L. Guazzotto[1,a] and R. Betti[2]
[1]Physics Department, Auburn University, Auburn, Alabama 36849, USA
[2]Department of Mechanical Engineering, University of Rochester, Rochester, New York 14627, USA

(Received 13 July 2015; accepted 11 August 2015; published online 3 September 2015)

The effects of finite macroscopic velocities on axisymmetric ideal equilibria are examined using the two-fluid (ions and electrons) model. A new equilibrium solver, the code FLOW2, is introduced for the two-fluid model and used to investigate the importance of various flow patterns on the equilibrium of tight aspect ratio (NSTX) and regular tokamak (DIII-D) configurations. Several improvements to the understanding and calculation of two-fluid equilibria are presented, including an analytical and numerical proof of the single-fluid and static limits of the two-fluid model, a discussion of boundary conditions, a user-friendly free-function formulation, and the explicit evaluation of velocity components normal to magnetic surfaces. © *2015 AIP Publishing LLC*.
[http://dx.doi.org/10.1063/1.4929854]

I. INTRODUCTION

Toroidal axisymmetric systems, such as tokamaks, are currently the main candidates for demonstrating a burning plasma in the laboratory. One of the cornerstones of our understanding of tokamak behavior is the study of their equilibrium properties. Based on experimental and theoretical results, it has been observed that macroscopic plasma rotation plays an important role in determining the behavior of the plasma. Equilibria of rotating plasmas have mostly been studied using single-fluid magnetohydrodynamic (MHD) models, see, e.g., Refs. 1–5. More recently, several authors have included the modification that will occur to the equilibrium if ions and electrons are described as two different fluids, instead of being considered as a single entity, see, e.g., Refs. 6–11. This line of research has been focused on axisymmetric plasmas.

The two-fluid model allows to differentiate the fluid properties of ions and electrons, in particular pressures, velocities, and in principle densities (even though the simplifying quasi-neutrality assumption neglects this effect). Since electron inertia is negligible with respect to ion inertia, plasma macroscopic mass flow is determined by ion velocities. An effect of this fact is that, contrary to the MHD case, plasma flow will be on surfaces that are not magnetic flux surfaces. As a consequence, there will in general be a finite plasma normal velocity to any magnetic surface, a fact which is not allowed in MHD theory. An additional fact worth mentioning (even though it is not further examined in this work) is that, contrary to MHD theory, two-fluid theory allows to distinguish how much current is separately carried by ions and electrons.[12]

The study of axisymmetric two-fluid equilibrium was pioneered by Steinhauer,[6] who first expressed the equilibrium problem in a differential form similar to the one used in this paper. A variational formulation was considered by Goedbloed[8] and Hameiri and coworkers.[10,13,14] Steinhauer was also the first author to highlight that a two-fluid equilibrium is a perturbation of a single-fluid one.[7] The same approach was later considered by Hameiri.[10] Remarkably, the problem of formally expressing the MHD equilibrium problem as a limit of the two-fluid one was not solved until recently.[10] Numerical solutions of the equilibrium problem are a challenging problem: the only code that implements a two-fluid equilibrium numerical solution is the one presented in Ref. 15. Applications to equilibrium reconstruction have been proposed,[12] but have not yet become a standard practice in tokamak research.

In the present work, we continue this latest line of research and introduce the numerical code FLOW2 for the solution of the two-fluid equilibrium problem. The code will be made freely available to the community, with the purpose of allowing other researchers to explore two-fluid effects on tokamak physics. For this reason, much emphasis is put on the flexibility of the code and its input and on the ease of use. Several sample applications are presented, both to standard aspect ratio tokamaks and to spherical tokamaks, to illustrate the properties of the system. The main innovations in our implementation and results are as follows. The code input is formulated in terms of "quasi-physical" free functions, which allow for an intuitive and user-friendly interface. It is proven that FLOW2 reproduces the analytical limits described below, emphasizing that the code is capable to handle a wide range of input conditions. The issue of boundary conditions is critically analyzed, and an original formulation of boundary conditions is implemented. Equilibria in regimes other than the traditional slow-poloidal flow one are calculated. Applications to both spherical tokamak and standard tokamak configurations are presented.

The paper is organized as follows. In Section II, the equilibrium equations are briefly derived. In Section III, the MHD (single-fluid) limit is examined, in conjunction with the definition of the input free functions, which is done paralleling the MHD definition. In Section V, details are provided on the approach for the numerical solution of the problem. In Section VI, spherical torus examples, with special reference

[a]Author to whom correspondence should be addressed. Electronic mail: luca.guazzotto@auburn.edu

to the national spherical torus NSTX, are shown. In Section VII, applications to standard aspect ratio tokamaks, in particular DIII-D, are shown. In Section VIII, a class of equilibria with high poloidal rotation is explored. In Section IX, possible effects of two-fluid physics on macroscopic tokamak stability are discussed. Finally, the results of the paper are summarized in Section X.

II. EQUATIONS

In this section, we briefly review the two-fluid equilibrium formulation. The two-fluid system of equations in the approximation described in this paper has been obtained by a number of authors, see, e.g., Refs. 6, 8, 16, 9, and 10. No matter the details of the derivation, all models start from the ideal two-fluid equilibrium equations, complemented by the low-frequency Maxwell equations

$$\nabla \cdot (n_j \underline{u}_j) = 0, \tag{1}$$

$$m_j n_j \underline{u}_j \cdot \nabla \underline{u}_j + \nabla p_j = -m_j n_j \nabla \Lambda + q_j n_j (\underline{E} + \underline{u}_j \times \underline{B}), \tag{2}$$

$$\nabla \cdot \underline{E} = \frac{1}{\epsilon_0} \sum n_j q_j (\simeq 0), \tag{3}$$

$$\nabla \times \underline{E} = 0, \tag{4}$$

$$\nabla \cdot \underline{B} = 0, \tag{5}$$

where all symbols have their usual meaning (n_j = species number density, $\underline{u}_j$ = species fluid velocity, m_j = species mass, p_j = species pressure, q_j = species charge, $\underline{E}$ = electric field, $\underline{B}$ = magnetic field, ϵ_0 = permittivity of free space, and j is the species label), with Λ being the gravitational potential, which will not be used in the applications described in this paper, but can be included in the derivation without any additional complication. It is also necessary to express the plasma current as

$$\underline{J} = \frac{1}{\mu_0} \nabla \times \underline{B} = \sum n_j q_j \underline{u}_j, \tag{6}$$

where μ_0 is the magnetic permeability of vacuum. From Eq. (4), it is also $\underline{E} = \nabla \Phi$. Moreover, an expression for enthalpy and a closure are needed for each species. As closures, we assume the existence of two conserved quantities (one per species) along the fluid motions

$$\underline{u}_{i,e} \cdot \nabla S_{i,e} = 0, \tag{7}$$

where $S_{i,e}$ are functions of pressures and densities. We work in cylindrical coordinates (R, φ, Z) and assume axisymmetry, $\frac{\partial}{\partial \varphi} = 0$.

For the derivation of the equilibrium system, we define

$$\underline{B} = \nabla \psi \times \nabla \varphi + F^* \nabla \varphi \quad F^* = F^*(R,Z) = RB_\varphi, \tag{8}$$

where the F^* notation is used to emphasize that, contrary to the classical Grad-Shafranov (GS) case, $B_\varphi R$ is not a flux function. From Eqs. (1) and (6), we write

$$n_j \underline{u}_j = \nabla C_j \times \nabla \varphi + G_j \nabla \varphi, \tag{9}$$

$$-\frac{1}{\mu_0} \Delta^* \psi \nabla \varphi + \frac{1}{\mu_0} \nabla F^* \times \nabla \varphi = \sum q_j G_j \nabla \varphi + \sum q_j \nabla C_j \times \nabla \varphi, \tag{10}$$

where $\Delta^* \psi \equiv R^2 \nabla \cdot [(\nabla \psi)/(R^2)]$. Eq. (9) holds because of axisymmetry; the quantities C_j and G_j will be defined shortly, after their physical meaning becomes clear. It is expedient to use the curl of the "extended" momentum $\mathcal{P}_j$ (the "generalized vorticity" of Ref. 10)

$$\underline{K}_j \equiv \nabla \times \mathcal{P}_j = \nabla \times (m_j \underline{u}_j + q_j \underline{A}), \tag{11a}$$

where $\underline{A}$ is the vector potential. Straightforward algebra gives

$$\underline{K}_j = q_j \left[\left(F^* - \frac{m_j}{q_j} \Delta^*_{n_j} C_j \right) \nabla \varphi + \nabla \Psi_j \times \nabla \varphi \right]. \tag{11b}$$

In Eq. (11b), $\Delta^*_{n_j} C_j \equiv R^2 \nabla \cdot [(\nabla C_j)(n_j R^2)]$ and

$$\Psi_j \equiv \psi + \frac{m_j G_j}{q_j n_j}, \tag{12}$$

which serves as a definition of G_j. Using the fact that $S_j = S_j(\Psi_j)$ due to Eq. (7), and writing

$$\nabla \left[m_j \frac{u_j^2}{2} + m_j \frac{\gamma_j}{\gamma_j - 1} S_j n^{\gamma_j - 1} + m_j \Lambda - q_j \Phi \right] \equiv \nabla H_j, \tag{13}$$

after some more straightforward algebra, we obtain the final form of the momentum equations

$$\nabla H_j - m_j \frac{n_j^{\gamma_j - 1}}{\gamma_j - 1} \frac{dS_j}{d\Psi_j} \nabla \Psi_j = \underline{u}_j \times \underline{K}_j, \tag{14}$$

where γ_j is the polytropic index of each species (the isothermal closure is recovered taking the limit $\gamma_j \to 1$), and explicit expressions for species enthalpies have been introduced. The $\nabla \varphi$, $\underline{K}_j$ and $\nabla \Psi_j$ components of Eq. (14) give, respectively,

$$C_j = C_j(\Psi_j), \tag{15}$$

$$H_j = H_j(\Psi_j), \tag{16}$$

$$m_j \nabla \cdot \left(\frac{\phi_j}{n_j} \frac{\nabla \Psi_j}{R^2} \right) \phi_j - q_j \frac{F^*}{R^2} \phi_j + \frac{q_j G_j}{R^2} = n_j \left(\frac{dH_j}{d\Psi_j} - m_j \frac{n_j^{\gamma_j - 1}}{\gamma_j - 1} \frac{dS_j}{d\Psi_j} \right), \tag{17}$$

where $\phi_j(\Psi_j) \equiv C_j'(\Psi_j)$ (not to be confused with Φ, introduced earlier to denote the electric potential).

We complete the derivation by introducing two standard assumptions: (1) we neglect electron inertia, and (2) we assume quasi-neutrality. By taking the limit of large plasma parameters, two-fluid effects related to finite Debye length[8,17] are neglected in this paper, as is common practice in two-fluid equilibrium theory. Setting for convenience $n_e = n_i \equiv n$, $\Psi_i \equiv \Psi$, $\Psi_e = \psi$ [setting $m_e = 0$ in Eq. (12)],

summing over the two species the $\underline{K}_j$ components of the momentum equations and after some straightforward algebra, we obtain the expression for the electric field

$$\underline{E} = -\frac{\nabla p_e}{en} - \underline{v} \times \underline{B} + \frac{\nabla \times \underline{B} \times \underline{B}}{e\mu_0 n}, \tag{18}$$

and the summary of the equilibrium equations

$$\underline{v} = \underline{u}_i = \frac{1}{n}(\phi \nabla \Psi \times \nabla \varphi + G_i \nabla \varphi)$$
$$= \frac{\phi}{n}\nabla\Psi \times \nabla\varphi + \frac{e}{m_i}(\Psi - \psi)\nabla\varphi, \tag{19}$$

$$F^* = B_\varphi R = \mu_0 e(C_i - C_e) + F_0, \tag{20}$$

$$\frac{v^2}{2} + \frac{\gamma_i}{\gamma_i - 1} S_i n^{\gamma_i - 1} + \frac{\gamma_e}{\gamma_e - 1} S_e n^{\gamma_e - 1} + \Lambda$$
$$= \frac{1}{m_j}\left[H_i(\Psi) + H_e(\psi)\right], \tag{21}$$

$$\phi m_i \nabla \cdot \left(\frac{\phi}{n}\frac{\nabla\Psi}{R^2}\right) - e\frac{\phi F^*}{R^2} + \frac{e^2 n}{m_i R^2}(\Psi - \psi)$$
$$= n\left(\frac{dH_i}{d\Psi} - m_j \frac{n^{\gamma_i - 1}}{\gamma_i - 1}\frac{dS_i}{d\Psi}\right), \tag{22}$$

$$\Delta^*\psi + \frac{e^2\mu_0 n}{m_i}(\Psi - \psi) + e\mu_0 F^* \phi_e$$
$$= -\mu_0 R^2 n\left(\frac{dH_e}{d\psi} - m_j \frac{n^{\gamma_e - 1}}{\gamma_e - 1}\frac{dS_e}{d\psi}\right). \tag{23}$$

The definitions

$$\phi \equiv \frac{dC_i}{d\Psi}, \quad \phi_e \equiv \frac{dC_e}{d\psi}, \tag{24}$$

have been used. In the following, we will use the fact that $v_\varphi \propto \delta\psi = \Psi - \psi$, as seen from Eq. (19), often. In order to solve the system of equations (21)–(23), it is necessary to assign the free functions $C_i(\Psi)$, $C_e(\psi)$, $H_i(\Psi)$, $H_e(\psi)$, $S_i(\Psi)$, $S_e(\psi)$. This is a delicate task, since there is in principle no guarantee that an equilibrium will exist for an arbitrary set of input free functions (indeed, direct experience shows that the opposite is much more likely to be true). It is not entirely clear at this stage what makes the choice of input functions for the two-fluid system more challenging than for the single-fluid equilibrium with flow problem and much more so than for the static equilibrium case. One may conjecture that the added physics more strongly constrains the input by limiting the space of self-consistent input combinations. On the other hand, since the relaxation method used for the solution (see Section V) resembles a time-dependent evolution, one may also conjecture that the lack of convergence indicates the presence of strong instabilities in the system, rather than its lack of equilibrium. The investigation of this issue is postponed to future work. The approach followed in the implementation of FLOW2 and for the remainder of this work is to assign a set of "intuitive" or "quasi-physical" functions[18] in a fashion similar to what is done for the code FLOW.[5] It is convenient to do this starting from the derivation of the MHD limit of the two-fluid system of equilibrium equation, which gives useful guidance on the way to assign the input. This is carried out in Secs. III and IV.

III. THE MHD LIMIT

The MHD reduction of the two-fluid equilibrium formulation was an open problem for several years, see, e.g., Ref. 7 and was only recently solved by Hameiri.[10] Here, we briefly sketch a derivation formally different from Hameiri's variational one, even if equivalent to it. The MHD limit is recovered from the two-fluid model by taking the limit $\delta\psi = \Psi - \psi \to 0$ or equivalently the vanishing ion skin depth limit[7]

$$d_i = \sqrt{\frac{m_i}{ne^2\mu_0}} \to 0. \tag{25}$$

The crucial element of the derivation is in the definition of Bernoulli functions, Eq. (13). The largest term on the left-hand side of Eq. (13) is the electric potential Φ. As stated by Hameiri, if $q_i = 1$, $H_e(\psi)$ and $H_i(\Psi)$ are to lowest order (in a d_i expansion) the same function up to a sign. When calculating the single-fluid MHD limit, all terms of order $\delta\psi \equiv \Psi - \psi$ can be ignored, *except* the terms multiplying the electric field. Notice that

$$\Phi = \Phi_{SF}(\psi) + \Phi_{TF}, \tag{26}$$

with $\Phi_{TF} \ll \Phi_{SF}$, where the subscripts refer to the single- and two-fluid parts. From single-fluid theory[1]

$$\Omega(\psi) = \frac{d\Phi_{SF}(\psi)}{d\psi}. \tag{27}$$

We first recover the MHD expression for the toroidal field, by following Ref. 7. In order to satisfy the requirement that B_φ be of order 1 (in terms of the expansion parameters $\delta\psi$ or ion skin depth), it is useful to define

$$C_i(\Psi) = \int_0^\Psi \phi(x)dx, \tag{28}$$

$$C_e(\psi) = \int_0^\psi \phi(x)dx - \frac{F(\psi)}{e\mu_0}, \tag{29}$$

where the second term in Eq. (29) is one order smaller than the first one. Notice that (obviously) $\phi(x)$ is the same $\phi(x)$ defined by Eq. (24). We absorb the F_0 constant of Eq. (20) in C_e and write

$$C_i(\Psi) \simeq \int_0^\psi \phi(x)dx + \phi(\psi)\delta\psi. \tag{30}$$

To complete the derivation of the lowest order expression for B_φ, we also need the *lowest order* toroidal velocity, which with the notation of the present document is written as

$$v_\varphi \simeq \frac{\phi(\psi)F^*}{nR} + R\Omega(\psi). \tag{31}$$

This is easily recovered from the lowest-order part of Faraday's + Ohm's laws. Using Eqs. (28)–(30), accompanied by Eq. (31) in Eq. (10), the MHD expression for the toroidal field is also consistently and trivially recovered

$$B_\varphi R = \frac{F(\psi) + \mu_0 m_i R^2 \phi(\psi)\Omega(\psi)}{1 - M_{Ap}^2}, \tag{32}$$

where

$$M_{Ap}^2 = \mu_0 m_i \frac{\phi^2}{n}\frac{|\nabla\Psi|^2}{|\nabla\psi|^2}. \tag{33}$$

(observe that the function ϕ has the same meaning in the present paper and in MHD equilibrium formulations, e.g., in Refs. 5 and 1, but different physical dimensions).

Next, we consider the Bernoulli equation, Eq. (21). Direct substitution using obvious definitions (e.g., $\gamma = \gamma_e = \gamma_i$, $S = S_e + S_i$) gives

$$m_i\frac{v^2}{2} + \frac{\gamma}{\gamma-1}Sn^{\gamma-1} + m_i\Lambda = H_e(\psi) + H_i(\psi) + \frac{dH_i}{d\psi}\delta\psi, \tag{34}$$

which using Eqs. (12), (26), and (27) reduces to the single-fluid limit

$$m_i\frac{v^2}{2} + \frac{\gamma}{\gamma-1}Sn^{\gamma-1} + m_i\Lambda - m_iR\Omega v_\varphi = H(\psi). \tag{35}$$

For the Grad-Shafranov equation, summing Eqs. (22) and (23) divided by $(-\mu_0 R^2)$ leads to

$$\overbrace{\nabla\cdot\left[\frac{1}{R^2}\left(\nabla\psi - \frac{\mu_0\phi^2 m_i}{n}\nabla\Psi\right)\right]}^{①} + \overbrace{\frac{e\mu_0 F^*(\phi-\phi_e)}{R^2}}^{②} + \overbrace{\mu_0 m_i\frac{\phi\phi'}{nR^2}|\nabla\Psi|^2}^{③}$$
$$= \mu_0 n\left(\overbrace{\frac{dH_i(\Psi)}{d\Psi} + \frac{dH_e(\psi)}{d\psi}}^{④} - \overbrace{\frac{n^{\gamma_i-1}}{\gamma_i-1}\frac{dS_i}{d\Psi} - \frac{n^{\gamma_e-1}}{\gamma_e-1}\frac{dS_e}{d\psi}}^{⑤}\right). \tag{36}$$

Simply replacing $\Psi \to \psi$ and defining $\Gamma_i + \Gamma_e = \Gamma$ for every function Γ gives most of the correct terms by inspection. Term ① reduces to

$$① = \nabla\cdot\left[\left(1 - M_{Ap}^2\right)\frac{\nabla\psi}{R^2}\right]. \tag{37}$$

Terms ③ and ⑤ are also trivial, giving

$$③ = m_i\mu_0\underline{v}_p\cdot\underline{B}\frac{d\phi}{d\psi} \quad \text{and} \quad n⑤ = \frac{n^\gamma}{\gamma-1}\frac{dS}{d\psi}, \tag{38}$$

(up to some difference in notation). Term ② requires some work and was correctly expressed by Steinhauer in Ref. 7. Using the results of Eq. (32), we can express term ② using the definitions Eqs. (24), (28), and (29)

$$\phi(\Psi) = \frac{dC_i(\Psi)}{d\Psi} = \frac{\partial C_i(\psi)}{\partial\psi} + \frac{\partial^2 C_i(\psi)}{\partial\psi^2}\delta\psi$$
$$= \phi(\psi) + \phi'(\psi)\delta\psi, \tag{39}$$

$$\phi_e(\psi) = \frac{dC_e(\psi)}{d\psi} = \phi(\psi) - \frac{F'(\psi)}{e\mu_0}. \tag{40}$$

Substitution into ② gives

$$② = \frac{B_\varphi}{R}\frac{dF}{d\psi} + m_i\mu_0 B_\varphi v_\varphi\frac{d\phi}{d\psi}. \tag{41}$$

Combining the terms derived so far, all terms in Eq. (19a) of Ref. 5 are recovered, except the term involving $H(\psi)$ and the term involving $nR\Omega'(\psi)v_\varphi$. We finally focus on the terms

$$n\left[\frac{dH_i(\Psi)}{d\Psi} + \frac{dH_e(\psi)}{d\psi}\right], \tag{42}$$

in the right-hand side. Using the same procedure as in Bernoulli equation leads to the following:

$$\frac{dH_i(\Psi)}{d\Psi} = \frac{dH_i(\Psi)}{d\psi} + \frac{d^2H_i(\Psi)}{d\psi^2}\delta\psi$$
$$= \frac{dH_i(\Psi)}{d\psi} + m_iR\frac{d\Omega(\psi)}{d\psi}v_\varphi, \tag{43}$$

the last term of which is exactly the term apparently missing in the combination of Eqs. (22) and (23). Defining (to lowest order, which is the only order needed)

$$H(\psi) = H_e(\psi) + H_i(\Psi) = H_e(\psi) + H_i(\psi), \tag{44}$$

completes the derivation. The derivation of the single-fluid limit is useful for drawing a parallel between the two- and single-fluid systems and expressing the input free functions through a different set of free functions, which we call "intuitive" or "quasi-physical" in a way similar to what is done in Refs. 18 and 5 for the single fluid system. This is done in Sec. IV.

IV. THE INTUITIVE SET OF INPUT FREE FUNCTIONS

We assign the six input free functions $[C_i(\Psi), C_e(\psi), H_i(\Psi), H_e(\psi), S_i(\Psi), S_e(\psi)]$ using quasi-physical free functions as is done for the single-fluid case.[5] Free functions are written starting from Bernoulli equation Eq. (21),

which was defined with dimensions of [mass × velocity^2] and not [velocity^2] as in FLOW. This explains the ion masses appearing in the definitions. Looking at Eq. (32), we can immediately write

$$F(\psi) = R_0 B_0(\psi). \tag{45}$$

In order to be able to recover the FLOW expressions of the free functions in the one-fluid limit, it is necessary to define a "sound speed" free function as

$$C_s^2(x) = \frac{\gamma_i P_i(x) + \gamma_e P_e(x)}{m_i D_{TF}(x)}. \tag{46}$$

For clarity, we indicate the two-fluid equivalent of FLOW's $D(\psi)$ with D_{TF}, since the latter has the dimensions of a number density, while the former has the dimensions of a mass density (we drop the subscript where there is no ambiguity). Based on Eq. (19), we can write $\phi(x)$ as is done in Ref. 5 for $\phi_{FLOW}(\psi)$

$$\phi(x) = \frac{1}{\sqrt{m_i}} \sqrt{[\gamma_i P_i(x) + \gamma_e P_e(x)] D_{TF}(x)} \frac{M_\theta(x)}{B_0(x)}. \tag{47}$$

For $\Omega(x)$, we can use the result of Eq. (27), which states that $\Omega_{\text{TWO FLUIDS}} = \Omega_{\text{FLOW}}$

$$\Omega(x) = \sqrt{\frac{\gamma_i P_i(x) + \gamma_e P_e(x)}{D_{TF}(x)}} \frac{M_\varphi(x) - M_\theta(x)}{R_0}. \tag{48}$$

Entropies have trivial expressions

$$S_j(x) = \frac{P_j(x)}{m_i [D_{TF}(x)]^{\gamma_j}}. \tag{49}$$

For $H_j(x)$, we need (1) the single-fluid electric potential

$$\Phi(\psi) = \int_0^\psi \Omega(x) dx, \tag{50}$$

where $\Omega(x)$ is given by Eq. (48), and (2) an additional term related to ion pressure, the meaning of which will become clear later

$$\Phi_P(\Psi) = \frac{1}{e} \int_0^\Psi \frac{1}{D_{TF}(x)} \frac{dP_i(x)}{dx} dx. \tag{51}$$

This allows us to write the Bernoulli functions

$$H_i(\Psi) = \frac{\gamma_i P_i(\Psi) + \gamma_e P_e(\Psi)}{D_{TF}(\Psi)} \left[M_\theta(\Psi) M_\varphi(\Psi) - \frac{M_\varphi^2(\Psi)}{2} \right] + \frac{\gamma_i}{\gamma_i - 1} \frac{P_i(\Psi)}{D_{TF}(\Psi)} + \int_0^\Psi \left[e\Omega(x) - \frac{1}{D_{TF}(x)} \frac{dP_i(x)}{dx} \right] dx, \tag{52}$$

and

$$H_e(\psi) = \frac{\gamma_e}{\gamma_e - 1} \frac{P_e(\psi)}{D_{TF}(\psi)} - \int_0^\psi \left[e\Omega(x) - \frac{1}{D_{TF}(x)} \frac{dP_i(x)}{dx} \right] dx. \tag{53}$$

Observe that if Ω is an angular frequency as in FLOW, there is no mass in front of the Ω terms in H_j. There is a subtlety in the definition of Eq. (52) that is worth pointing out. In short, it is necessary to define Eq. (52) as written in order to recover the MHD expression for the free functions, and not only for the equilibrium equations. The practical approach is to start from the one-fluid expression of the LHS of the Bernoulli equation, subtract the electron pressure, define the 0th order H_i, and then add back the electric field piece. Another way to look at it is that the 0th order piece of the electric field term should also enter independently to define H_i. Notice that we have set the gravitational potential Λ to 0 in order to more closely parallel the expressions in Ref. 5. In the expressions above, the free functions $D_{TF}(x)$, $P_i(x)$, $P_i(x)$, $M_\theta(x)$, $M_\varphi(x)$, and $B_0(x)$ are the new input free functions. The definitions of the free functions are summarized in Table I. The user-friendly, intuitive input free functions used in the definitions above are two quasi-pressures, $P_i(x)$ and $P_e(x)$, the quasi-toroidal magnetic field $B_0(x)$, the quasi- toroidal and poloidal Mach numbers $M_\theta(x)$ and $M_\varphi(x)$, and the quasi-number density $D_{[TF]}(x)$. In the definitions above, "x" can be either ψ or Ψ and the word "quasi" refers to the fact that each physical quantity in the calculated equilibrium will be similar to the corresponding input free function and in fact reduce to it in the static cylindrical limit. In FLOW, the argument of every free function is normalized to the maximum value of ψ in the system, so that the numerical value of the independent variables in free function definitions is always between 0 and 1. The same approach is used in FLOW2. Since several free functions are used as functions of either ψ or Ψ, arguments are normalized to the largest of the two (typically Ψ for the runs in the present work).

Before proceeding with the details of the implementation and results of equilibrium calculations, it is appropriate to close the discussion of the MHD limit of the two-fluid system with a numerical verification of the analytical result. This is done by running a series of realistic DIII-D (Refs. 19 and 20) like equilibria. Each equilibrium in the series is run in both single- and two-fluid descriptions. Each equilibrium

TABLE I. Summary of free-function definitions in FLOW form.

Function	Definition
$F(\psi)$	$R_0 B_0(\psi)$
$\phi(x)$	$\sqrt{\frac{[\gamma_i P_i(x) + \gamma_e P_e(x)] D(x)}{m_i}} \frac{M_\theta(x)}{B_0(x)}$
$\Omega(x)$	$\sqrt{\frac{\gamma_i P_i(x) + \gamma_e P_e(x)}{m_i D(x)}} \frac{M_\varphi(x) - M_\theta(x)}{R_0}$
$H_i(\Psi)$	$\frac{\gamma_i P_i(\Psi) + \gamma_e P_e(\Psi)}{D(\Psi)} \left[M_\theta(\Psi) M_\varphi(\Psi) - \frac{M_\varphi^2(\Psi)}{2} \right] + \frac{\gamma_i}{\gamma_i - 1} \frac{P_i(\Psi)}{D(\Psi)} + \int_0^\Psi \left[e\Omega(x) - \frac{1}{D(x)} \frac{dP_i(x)}{dx} \right] dx$
$H_e(\psi)$	$\frac{\gamma_e}{\gamma_e - 1} \frac{P_e(\psi)}{D(\psi)} - \int_0^\psi \left[e\Omega(x) - \frac{1}{D(x)} \frac{dP_i(x)}{dx} \right] dx$
$S_j(x)$	$\frac{P_j(x)}{m_i [D(x)]^{\gamma_j}}$

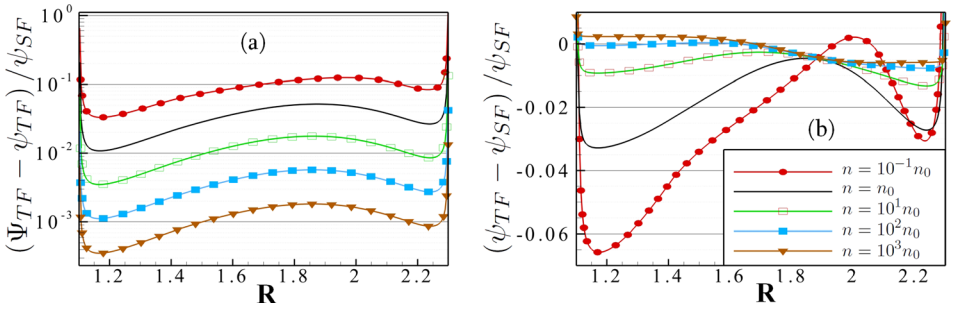

FIG. 1. Comparison between single- and two-fluid equilibrium. (a) Relative difference between Ψ and ψ in a two-fluid equilibrium shown in log scale as a line cut along the midplane. Differences are normalized to the single-fluid values of ψ for five different densities. (b) Relative difference between single- and two-fluid values of ψ shown in linear scale as a line cut along the midplane. Differences are normalized to the single-fluid values of ψ for five different densities. Same colors correspond to the same equilibrium in the two panes of the figure.

in the series has the same input free functions, except for the free function $D_{[TF]}$ controlling the density, which is increased by a factor of 10 going from one equilibrium to the next. As shown by Equation (25), a 10-fold increase in density corresponds to a reduction of the ion skin depth d_i by a factor of $\sqrt{10}$. Numerical results are shown in Fig. 1.

Figure 1(a) shows the relative difference between Ψ and ψ for two-fluid equilibria with five different input densities. Results are normalized to the single-fluid local values of ψ; the single-fluid equilibrium is also recomputed for each level of density for consistency, even though changing the input "quasi-density" free function does not modify the equilibrium. Results are shown in logarithmic scale with a line cut along the midplane. As expected, the difference decreases for increasing density. Moreover, the decrease is approximately one order of magnitude for each two orders of magnitude increase of the density, as expected from Eq. (25). The higher difference at the edge is due in part to the fact that edge values are close to 0 and in part to boundary condition issues, to which we will come back in Section V. Next, Fig. 1(b) shows a similar plot, but for the difference between the "magnetic" ψ in the two- and single-fluid case. Results are similar to the ones shown in Fig. 1(a): error decreases with increasing density. Since in this case the difference changes sign in the plasma, the plot uses a linear scale. The larger relative error at the edge is due to boundary condition issues. Also, since ψ (both single- and two-fluid) approaches 0 at the edge, the relative error appears large for numerical reasons, even though the actual difference is small.

In summary, in this section, it was shown that (1) ideal MHD is the single-fluid limit of the two-fluid system considered in this work and (2) the equilibrium results obtained by the numerical code FLOW2 approach single-fluid equilibrium results in the appropriate limit. This result also constitutes a solid benchmark for FLOW2. Details about the code are given in Sec. V.

V. NUMERICAL SOLUTION

The numerical implementation of FLOW2 is based on the SOR (successive over-relaxation) multi-grid, red-black algorithm used in FLOW. A Cartesian grid in cylindrical coordinates (R, φ, Z) is used (φ is the ignorable coordinate). Equations (21)–(23) are solved iteratively one at a time. Some manipulations are done to improve the convergence and numerical properties of the system. It is known that not all terms in Eqs. (22) and (23) are formally of the same order.[6,7,10] In particular, terms containing the difference between Ψ and ψ are the product of a large term and a small one and may create issues in the numerical solution. The approach that was found to be successful requires the following steps:

(1) Solve the sum of Eqs. (22) and (23), i.e., Eq. (36), for ψ (this eliminates all formally large terms).
(2) Solve Eq. (22) for v_φ, i.e., $\delta\psi = (\Psi - \psi)$ instead of Ψ (see Ref. 15).
(3) Solve Eq. (21) for n after obtaining v_φ from Eq. (22) (densities inside the differential operator are evaluated using the previous iteration, so that the equation remains algebraic); this makes the Bernoulli equation like the one in the single-fluid case.

Differently from Refs. 15 and 12, we do not use an analytic solution for n and adopt the same bracketing and solution search approach used in FLOW. This is done because Eq. (21) in general has more than one solution. The approach in Refs. 15 and 12 corresponds to always choosing the same ("heaviest") solution. Steps 1–3 above are repeated on each grid until convergence, defined by a required reduction of the global error in each of the differential equations. After convergence the code proceeds to the next, finer grid. The initial guess for the first grid is given by the converged MHD solution on the same grid and with the same input free functions. The variables ψ and n are initialized from the MHD ones, while Ψ is initialized from v_φ.

The input free functions $D_{TF}(x)$, $P_i(x)$, $P_e(x)$, $M_\theta(x)$, $M_\varphi(x)$, and $B_0(x)$ can have any desired shape. Some default polynomial shapes are implemented, but in practice it is usually more convenient to assign the input through numerical tables (arguments are normalized to the largest of the maximum values of ψ and Ψ). As already mentioned, in general, there is no guarantee that an equilibrium will be found for any given set of free functions. Indeed, the input is much more "delicate" than its one-fluid equivalent: if it is relatively easy to find a functioning input for FLOW, the task is quite more challenging for FLOW2. Part of the issue is related to the boundary conditions.

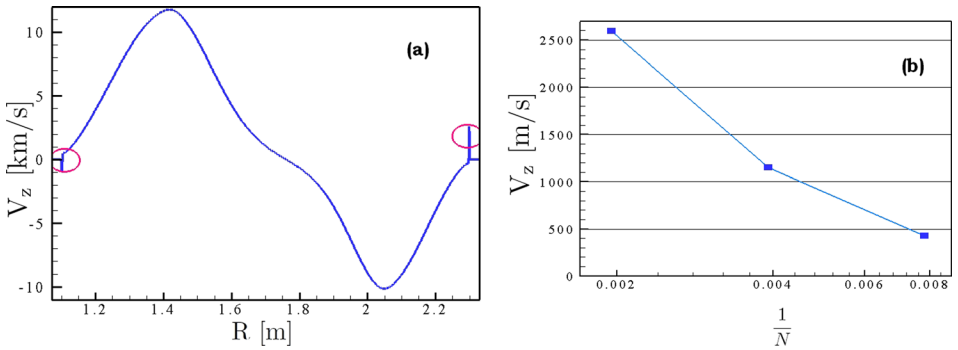

FIG. 2. (a) Poloidal velocity along the midplane for a "p300 k" BC and a resolution of 512×512 points. Unphysical edge peaks in poloidal velocity are circled in red. (b) Poloidal velocity edge peak value on the outer midplane as a function of resolution. The code does not converge for finer grids.

Plasma boundary in FLOW2 is defined in the same way as in (the current version of) FLOW. Some default analytical shapes are implemented, and tabulated values for the boundary shape are also allowed. Therefore, any desired shape can be assigned for the boundary. Since the grid is Cartesian, boundary ψ values are assigned in FLOW using linear interpolations: values just outside the boundary are determined so that the value of ψ at the intersection between the boundary curve and the normal to the boundary through the external point is equal to the required value, typically $\psi = 0$, even though in principle it is not necessary to assign the boundary conditions on a magnetic surface (this property has been used in the past for calculating free-boundary equilibria).

The same approach is used in FLOW2, but with an important modification regarding Ψ. For simplicity, in the present work, we will assume that the plasma boundary corresponds to a magnetic surface (the last closed flux surface, LCFS), where we set $\psi = 0$ for convenience. However, in general, there is no reason why the LCFS should also be a surface of constant Ψ. As expressed in Eq. (12), on a magnetic surface the value of Ψ will vary due to the fact that the toroidal velocity is varying. If the plasma density at the edge was known, one could obtain a self-consistent boundary condition by assigning v_φ on the boundary, which is typically finite in experiments, using Eq. (19). On the other hand, still using Eq. (19), one may want to also, or instead, assign the poloidal velocity on the boundary, and thus the gradient of Ψ rather than its value. Ideally, it could be desirable to assign both toroidal and poloidal velocity, but this is not allowed by the elliptic characteristic of the problem (unless the poloidal flow vanishes). All the results contained in this work are obtained in the elliptic region of the system given by Eqs. (19)–(22). The issue of ellipticity of the equilibrium equations with flow is discussed in Refs. 21 and 22. Coming back to boundary conditions, the approach that was implemented is the following. An approximate toroidal velocity is determined by using the MHD expression Eq. (31) and edge values for free functions instead of the corresponding physical quantities (e.g., $D_{TF}(0)$ instead of n). Since the first term in Eq. (31) is proportional to the plasma sound speed, which is small at the edge in the equilibria considered in the remainder of this paper, in practice one only needs to assign $\Omega_{edge} \simeq \Omega(0)$. Setting $v_\varphi = v_\varphi^{(MHD)}$ at the edge, i.e., $\Omega_{edge} = \Omega(0)$ is in general sufficient to obtain converged equilibria, but an accurate solution requires an iterative approach, in which the correct boundary condition is part of the solution of the problem.

The issue should not be underestimated. This is highlighted in Fig. 2, which shows results obtained for a DIII-D like equilibrium with an arbitrary boundary condition for Ψ, intentionally set to a value not consistent with the input. In the run, $\Omega_{edge} = 3 \times 10^5$ instead of the free-function value $\Omega(0) = -4.4 \times 10^3$; we indicate this run as "p300 k." Similar runs with other, positive or negative, large values of Ω_{edge} were computed, with similar results. Figure 2(a) shows the poloidal velocity profile along the midplane (on the midplane, $V_p = V_z$) for the maximum resolution used in the runs, 512×512 points. The velocity peak on the last grid point before the boundary is highlighted with a red circle. A similar peak for V_p is found in every boundary point in the grid. Figure 2(b) shows the height of the peak in the outboard midplane for different grid resolutions, showing an increase of the peak height with increasing resolution. The code will not converge with higher resolutions, because the poloidal velocity at the edge (proportional to $\nabla\Psi$ and thus related to ∇v_φ) becomes so large that a solution of the Bernoulli equation cannot be found.

After concluding the discussion of formulation and code implementation, we proceed with some numerical results.

VI. NSTX EQUILIBRIA

In the present section, the code FLOW2 is applied to NSTX[23] equilibrium calculations. Since high toroidal velocities are routinely obtained in NSTX and the difference between ψ and Ψ is proportional to the toroidal velocity, NSTX plasma is an excellent test bed for verifying the importance of two-fluid effects. Several equilibria with different inputs were calculated and only a selected subset is shown in the present work. The starting point for our calculations is an EFIT[24] static single-fluid reconstruction for shot 138146. FLOW2 implementation allows arbitrary input as numerical tables for any input free function, so the free functions B_0 and all quasi-pressure are entered as numerical tables. Single-fluid quasi-pressure is divided between ions and electrons. To prove the versatility of the implementation, the pressure is divided unevenly, with a larger fraction being assigned to the electrons at the edge and to the ions in the core. Toroidal frequency is extracted from experimental measurements and entered as input in the calculations also as a numerical table. Since the purpose of the present work is to show the capabilities of the new code FLOW2, we start by considering the effect of finite rotation at the plasma edge. This is highlighted in Fig. 3. The figure was obtained from a

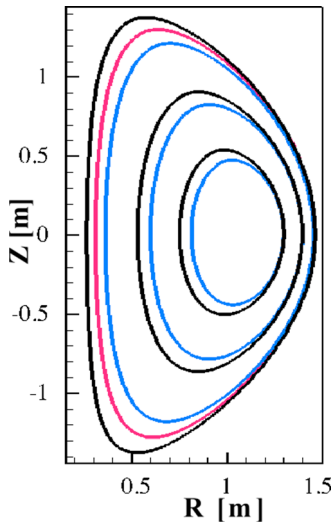

FIG. 3. Constant ψ (black) and Ψ (blue) surfaces for an NSTX equilibrium. A constant Ψ surface that crosses the plasma boundary is shown in red.

numerical equilibrium with 256 grid points in each direction. An adiabatic closure is used for both ions and electrons. A few magnetic surfaces ($\psi = \text{const.}$) and flow surfaces ($\Psi = \text{const.}$) inside the plasma are shown, in black and blue, respectively. For the purpose of illustration, surfaces that are tangential in the outer midplane are plotted, showing the difference between the two sets of surfaces anywhere else in the plasma. A "special" flow surface is shown in red: this surface crosses the plasma boundary (assigned from input). Thus, if the plasma is surrounded by a conforming wall, all plasma between the outmost blue (Ψ) surface and the outmost black (ψ) surface will stream directly into the wall. If we assume that the plasma streaming into the wall is absorbed or neutralized, there will be no plasma between the outmost blue and black curves, so the actual plasma boundary will be the outmost blue curve and not the outmost magnetic surface. If instead there is an X-point with an open-field-line vacuum region outside the $\psi = 0$ curve and the edge toroidal velocity is finite, it is not obvious what constitutes the plasma edge, as outer "flow" surfaces will cross the LCFS and be in part in the closed-field-line region and in part in the open-filed-line region. This is left as an open question, with the only firm point being the case of no edge toroidal velocity, for which the $\psi = 0$ and $\Psi = 0$ surfaces coincide and univocally define the plasma edge.

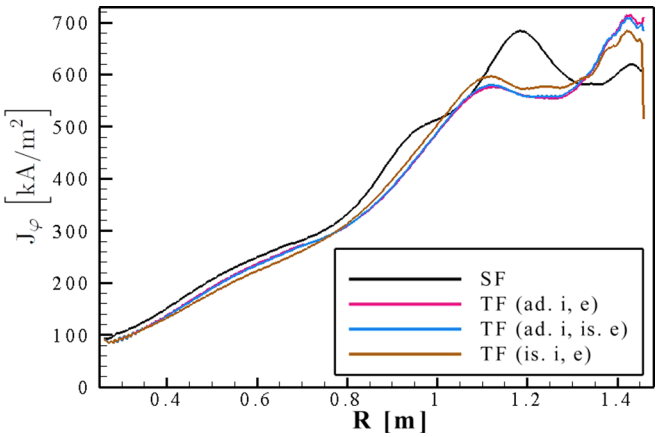

FIG. 4. Current density profiles along the midplane for single- (black) and two-fluid (color) equilibria. Adiabatic and isothermal closures are used for ions and electrons.

The next issue that is explored is the importance of the closure equation. The same equilibrium calculation is repeated four times: first, as a single-fluid, adiabatic equilibrium; second, as a two-fluid equilibrium with adiabatic ions and electrons; third, using adiabatic ions and isothermal electrons; and fourth, using isothermal ions and electrons. All equilibria have the same (smooth) input free functions obtained from an EFIT equilibrium reconstruction provided by Dr. Bortolon. In particular, a smooth profile is assigned for the rigid toroidal rotation $\Omega(\psi)$, resulting in a maximum toroidal Mach number $M_t = V_\varphi / C_s \sim 0.8$. Other relevant data are $\beta_t = 2\mu_0 \langle p \rangle / B_\varphi^2 \sim 0.11$, $I_p \sim 750k\,\text{A}$ (values change slightly between equilibria). The results of the different calculations are compared in Figs. 4 and 5. The first figure shows the one-dimensional plot along the mid plane of the plasma current density for all equilibria. The single-fluid equilibrium is in black, the other curves show the two-fluid results with ions and electrons both adiabatic (red), isothermal electrons and adiabatic ions (blue), and both species isothermal (brown). Results are qualitatively similar, but some differences are noticeable. First, the two-fluid equilibria have smaller current density in the inboard part of the plasma. Second, larger currents (corresponding to larger gradients) are obtained at the outboard edge of the plasma (note that a large edge current is obtained also with the single-fluid model and that this is typical for NSTX equilibria and not specific to the equilibrium under consideration). The single-fluid equilibrium also has a larger current peak near the magnetic axis. One should be careful in drawing conclusions such as "two-fluid equilibria will have larger edge currents" from these results. The real take home statement is that different (current) profiles are obtained if one uses the two-fluid model or the single-fluid one; if the purpose is to reproduce an equilibrium with a given current profile, one should use different inputs (hence the need for a two-fluid reconstruction code[12]). It may appear from Fig. 4 that the choice of closure for the two species does not have any importance, as all current density curves for two-fluid equilibria are rather similar. In fact, closure effects on macroscopic equilibrium properties become relevant only with high rotation, even in the single-fluid case.[25] One important effect of the choice of closure is seen in Fig. 5, which shows isothermal surfaces for the series of equilibria considered in this section. Two-dimensional constant temperature curves are shown for the various equilibria at fixed level, either 1 and 2 keV (for the single-fluid equilibrium) or 0.5 and 1 keV for each species. Ion temperatures are shown in blue, electrons' in red. The three subplots correspond to the three different choices made for the closures: both species adiabatic (a), isothermal electrons and adiabatic ions (b), and both species isothermal (c). Due to both the uneven way temperature is divided between ions and electrons and to the difference between single and two-fluid equilibria, single and two-fluid curves are not coincident in any of the considered equilibria. Moreover, the curves change with different choices for the closure. It is

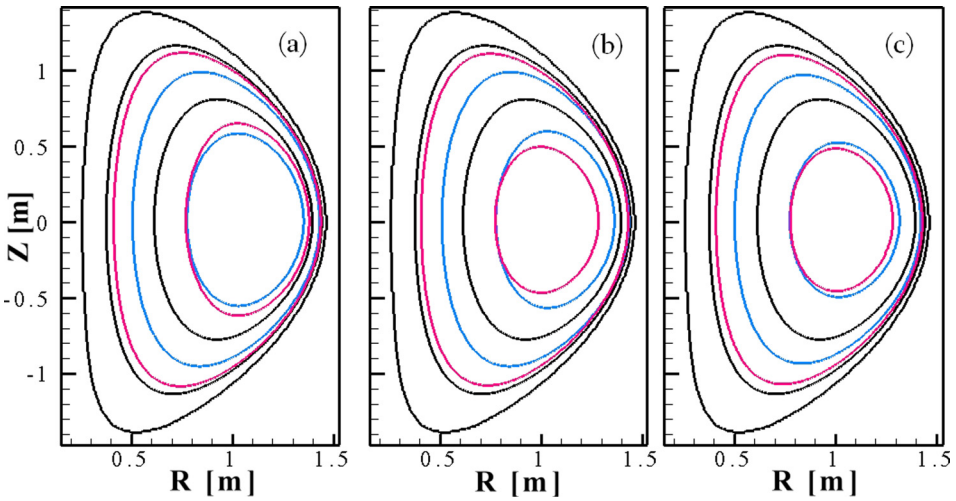

FIG. 5. Isothermal surfaces for single- (black) and two-fluid (color) equilibria. Single-fluid curves are at 1 and 2 keV, two-fluid ones at 0.5 and 1 keV for each species. In pane (a), both species are isentropic, in (b) ions are isentropic and electrons isothermal, and in (c) both species are isothermal. Ions are in blue, electrons in red.

worthwhile to remember that all "free" functions in fluid equilibrium calculations are in reality determined by transport. Even though it is in principle possible to calculate equilibria with completely arbitrary profiles for the free functions, the user should be careful in checking that the results do not violate intuitive transport principles, in particular, in the two-fluid case.

We now proceed to consider some standard aspect ratio tokamak results.

VII. DIII-D EQUILIBRIA

We now explore equilibria in the standard-tokamak range, with lower β and higher aspect ratio. Direct calculation shows that these are less challenging from a numerical point of view, in the sense that it is easier to construct a well-converging equilibrium and that the input can be modified fairly arbitrarily without convergence issues. We consider a "standard" DIII-D equilibrium with smooth analytic input free functions and examine different levels of rotation to highlight a point that has not yet been discussed. Some of the main plasma parameters are $I_p \simeq 1$ MA, $\beta_t \simeq 0.01$, and $q^* \simeq 2.5$ (values change slightly between different equilibria). We start with a "nominal" level of rotation and calculate a series of equilibria with the input free functions related to plasma rotation (M_φ and M_θ, see Table I) multiplied by factors from 0.001 to 2. The "nominal" equilibrium has a maximum toroidal Mach number $M_t \equiv V_\varphi/C_S \simeq 0.66$, already a high rotation for DIII-D. It is trivial to extend the calculation to lower rotations, but there is an upper limit to the level of toroidal and (especially) poloidal rotation that can be included in the system.

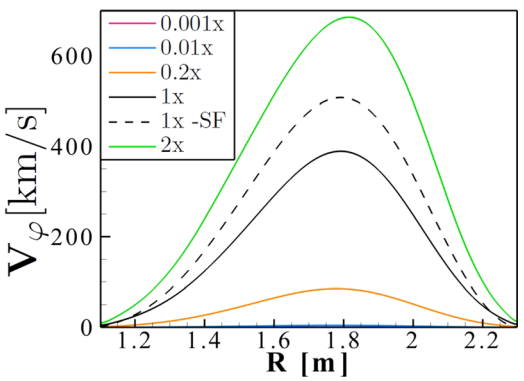

FIG. 6. Toroidal velocity (in km/s) in DIII-D two-fluid equilibria. The different colors correspond to nominal rotation (black) and nominal rotation multiplied by 0.001 (red), 0.01 (blue), 0.2 (orange), and 2 (green). The single-fluid equilibrium with nominal rotation is included for reference.

We consider the toroidal rotation shown in Fig. 6. The figure shows a line cut along the midplane of the velocity profile for five different level of rotation (all in the two-fluid model, except for the nominal rotation, which is also shown for the single-fluid case). The black curve corresponds to the nominal rotation level, while the color curves show the results for nominal rotation multiplied by 0.001 (red), 0.01 (blue), 0.2 (orange), and 2 (green). The resulting rotation is what one would have expected: the equilibria with $0.2\times$ and $2\times$ nominal rotation have a rotation profile that is approximately $1/5$ and twice the nominal one, and the equilibria with 1% and 0.1% of the nominal rotation in the input have a very small level of calculated rotation (indistinguishable in the scale of Fig. 6). This should not be surprising, but there is a subtlety in the formulation that is required to correctly model the low rotation case, which is highlighted next.

The static case is obtained by writing Eq. (22) and considers its limit for vanishing free functions M_φ and M_θ (compare to Table I). By setting $M_\theta = 0$, one immediately obtains

$$\frac{e^2 n}{m_i R^2}(\Psi - \psi) = n\left(\frac{dH_i}{d\Psi} - \frac{n^{\gamma_i - 1}}{\gamma_i - 1}\frac{dS_i}{d\Psi}\right), \tag{54}$$

which can still be solved for Ψ (in fact, the terms that vanish for no poloidal rotation are always taken to the right hand side in FLOW2's numerical approach, see Section V). Further setting $M_\varphi = 0$, one obtains

$$\frac{e^2}{m_i R^2}(\Psi - \psi) = \frac{\gamma_i}{\gamma_i - 1}\frac{d}{d\Psi}\left[\frac{P_i(\Psi)}{D(\Psi)}\right] - \frac{1}{D(\Psi)}\frac{dP_i(\Psi)}{d\Psi} - \frac{n^{\gamma_i - 1}}{\gamma_i - 1}\frac{d}{d\Psi}\left[\frac{P_i(\Psi)}{D(\Psi)^{\gamma_i}}\right]. \tag{55}$$

If one now allows that the $M_\theta = M_\varphi = 0$ equilibrium under consideration does indeed correspond to a static equilibrium

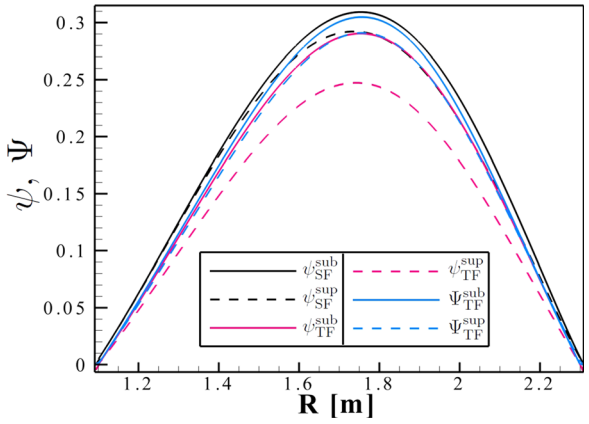

FIG. 7. ψ and Ψ profiles for single- (black) and two-fluid (color) subsonic (solid lines) and supersonic (dashed lines) equilibria. For the two-fluid equilibria, magnetic flux ψ is in red, flow stream function Ψ in blue.

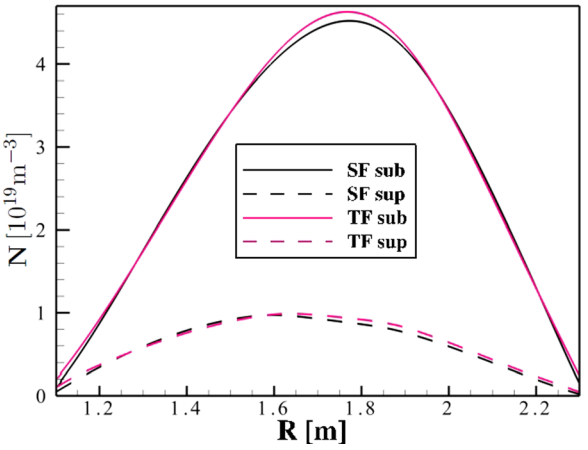

FIG. 8. Number density profiles for single- (black) and two-fluid (color) subsonic (solid lines) and supersonic (dashed lines) equilibria.

and therefore that $\Psi = \psi$ [recall that the toroidal velocity v_φ is proportional to $(\Psi - \psi)$], the Bernoulli equation Eq. (21) gives $n = n(\psi) = D(\psi)$. Substitution in Eq. (55) shows that Eq. (55) is automatically satisfied. The subtlety consists in the expression of the electric potential piece of the Bernoulli functions $H_i(\Psi)$ and $H_e(\psi)$ (the term under the sign of integration in Table I), which needs to include the electrostatic term P_i'/D, without which it would not be possible to balance Eq. (22) in the static case. Numerical results show that for vanishing rotation the plasma density is indeed a flux function (not shown).

Next, we investigate the importance of two-fluid effects in a different class of equilibria.

VIII. SUPERSONIC EQUILIBRIUM

We have so far considered only equilibria with relatively small poloidal flows, with the poloidal velocity smaller than the poloidal sound speed $(v_p < C_{sp} = C_s B_p/B)$. It is well known that in single-fluid equilibria with poloidal rotation, the Bernoulli equation can have more than one root for the plasma density, with each root corresponding to a different velocity. The two roots with the smaller velocity correspond to a subsonic and a supersonic root, as referred to the poloidal sound speed. In previous work by other authors, only the subsonic root was considered. Even though the slower poloidal rotation velocity is the most relevant one for tokamak equilibria, it is worthwhile to explore the possibility to obtain an equilibrium with rotation faster than the poloidal sound speed. This is easily accomplished in FLOW2 since the Bernoulli equation solver is built on the framework of the one developed for FLOW, which allows to select sub-, super-, or transonic equilibria.

For our investigation, we consider a "simple" set of free functions with smooth analytic profiles for a low-β equilibrium in DIII-D geometry. Standard DIII-D plasma shape is used. Since we are looking for an equilibrium with supersonic (with respect to the poloidal sound speed) poloidal flows over the whole plasma cross section, a wide profile is assigned for the free function M_θ, with M_θ being finite for any value of its independent variable. Four different equilibria are considered *with exactly the same input*: two single-fluid equilibria and two two-fluid equilibria, one subsonic and one supersonic for each model. For the reasons discussed earlier, the boundary conditions need to be modified for the two-fluid equilibria (different values of Ψ need to be assigned at the boundary for the subsonic and the supersonic equilibria). Results are shown in Figs. 7–9. All figures show line cuts along the mid plane.

First, Fig. 7 shows the magnetic flux ψ and the stream function Ψ for all equilibria (Ψ only for the two-fluid ones). Single-fluid results are shown in black, while for the two-fluid model ψ is in red and Ψ in blue. Subsonic profiles are shown with solid lines and supersonic ones with dashed lines. Several points can be observed from Fig. 7. In the subsonic case, the difference between the single- and two-fluid ψ is small (even though there is s slight difference in the position of the magnetic axis) and the difference between $\psi_{(TF)}$ and Ψ (solid color curves) is even smaller. Supersonic results are quite different from subsonic ones, more so in the two-fluid case than in the one fluid one. The difference between ψ and Ψ [proportional to the toroidal rotation velocity, see later Fig. 9(a)] also becomes very large (dashed color curves).

Next, we consider the density profiles. Single- and two-fluid profiles are quite similar, but not identical. The magnitude of the difference between the two models is similar in the two cases, but in the supersonic case there is a shift in the position of the maximum of the density (maxima are coincident in the subsonic case).

Next, we examine toroidal velocities, which are shown in Fig. 9(a). Profiles for the two models are fairly similar, for both the subsonic and the supersonic case, with slightly larger velocities for the single-fluid model (this is not a general result). There is an almost constant offset between the two models in the supersonic case. The two profiles for the subsonic case are also qualitatively similar, but they cross in the outer midplane, where the two-fluid value remains positive and the single-fluid one becomes negative. Observe that for all equilibria v_φ is finite at the plasma edge, meaning that for this input $\Psi \neq \psi$ must be assigned as boundary condition.

Finally, the poloidal velocity profiles are shown in Fig. 9(b). Once again profiles are rather similar, with the two-fluid model predicting on average slightly smaller velocities

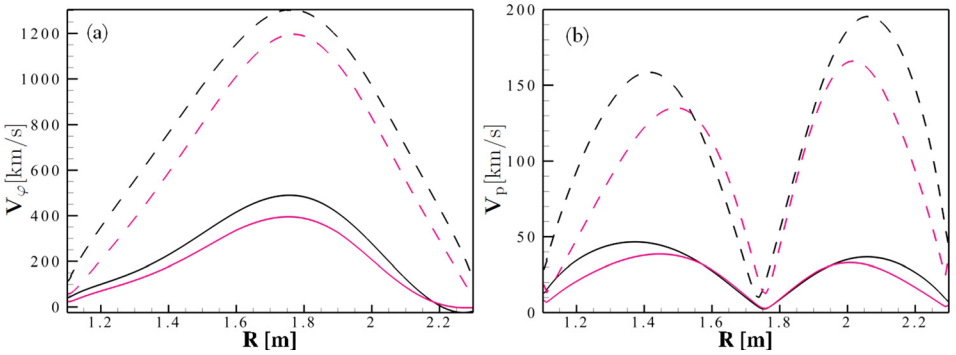

FIG. 9. Toroidal (a) and poloidal (b) velocity profiles (in km/s) for single- (black) and two-fluid (color) subsonic (solid lines) and supersonic (dashed lines) equilibria.

than the single-fluid one. The positions of the poloidal velocity maxima are different in the two models. In the supersonic case, the position of the velocity minimum is also different between the two models. As already observed for the toroidal velocity, differences between the two models are larger in the supersonic case.

The results in this section indicate that the difference between the one and the two-fluid models for equilibria with fast poloidal flows, even though still perturbative, is much larger than in the slow-rotation case.

IX. NORMAL VELOCITY COMPONENT

It was emphasized in Secs. I–VIII that the main macroscopic difference between MHD and two-fluid equilibria is the presence of a finite v_ψ, the component of plasma velocity normal to magnetic surfaces. The analysis of the effect of this new (with respect to MHD) element introduced by the two-fluid model will be the object of future work. In particular, it is conjectured that a finite v_ψ will have an effect on the linear properties of slow-growing unstable modes localized on magnetic (resonant) surfaces. A rich literature exists on the study of the effect of two-fluid physics on unstable modes, in particular, in the astrophysics field, see, e.g., Refs. 26–28, but also in tokamak physics, see, e.g., Refs. 29–36. Two-fluid equilibrium equations introduce a component of the velocity normal to magnetic surfaces (v_ψ), which can be important at resonant surfaces for localized modes. Even though the investigation of how two-fluid equilibrium properties may be relevant for macroscopic stability is deferred to future work, it is worthwhile to consider how this may be the case. This is done by calculating magnitude and shape of v_ψ for sample equilibria considered in this work.

The velocity component normal to a magnetic surface is calculated numerically as

$$v_\psi = \frac{\underline{v}_p \times \underline{B}_p}{|B_p|}. \tag{56}$$

What is immediately apparent from Eq. (56) is that v_ψ is always going to be a fraction of v_p, thus much smaller than the sound speed C_s in standard tokamak equilibria. Based on Eq. (56) it is also worth comparing the size v_ψ and v_p.

Some results for v_ψ and the ratio v_ψ/v_p are shown in Figs. 10 (for a subsonic DIII-D equilibrium) and 11 (for an NSTX equilibrium). Both figures show v_ψ (solid lines) and v_ψ/v_p (dotted lines with circular markers) as a function of the poloidal angle θ on three magnetic surfaces corresponding to three safety factor values, $q = 1$ or $q = 4/3$ (blue), $q = 3/2$ (red), and $q = 2$ (black). Since q on axis is larger than unity for the NSTX equilibrium, the value $q = 4/3$ is used for the NSTX plot. For the equilibria considered here, v_ψ is in the range of tens to hundreds of m/s, fairly small compared to other relevant velocities in the system. In the DIII-D case (Fig. 10), this is only a small fraction of v_p ($\lesssim 3\%$). However, v_ψ is a much larger fraction of v_p, up to more than 30% on the $q = 4/3$ surface for the NSTX case.

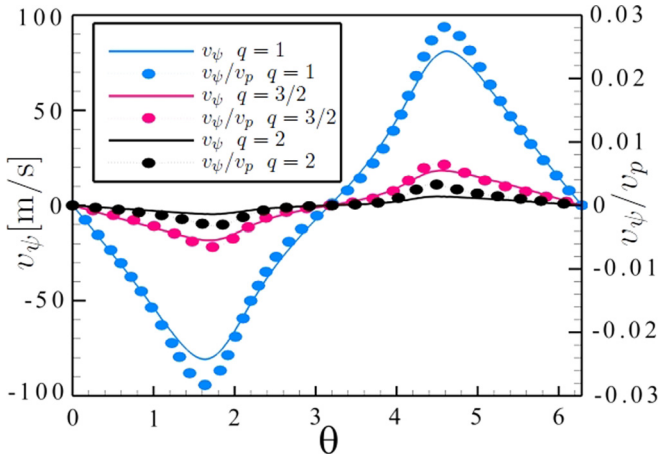

FIG. 10. Normal velocity v_ψ (solid lines) on three rational surfaces ($q = 1$, $q = 3/2$ and $q = 2$) in a DIII-D equilibrium. Ratios v_ψ/v_p are also plotted (dotted lines with circles). Resolution is 256 × 256 points.

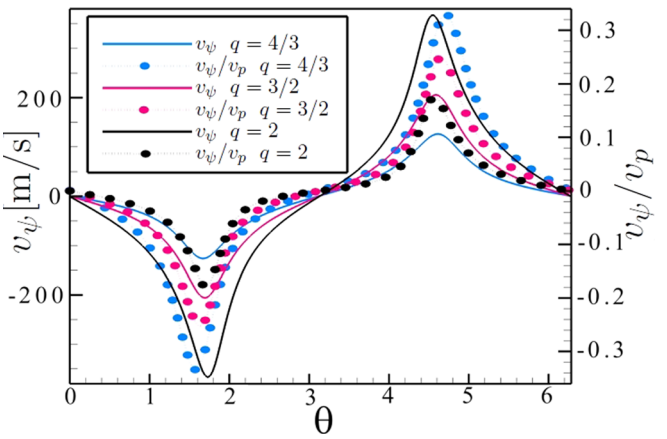

FIG. 11. Normal velocity v_ψ (solid lines) on three rational surfaces ($q = 4/3$, $q = 3/2$ and $q = 2$) in an NSTX equilibrium. Ratios v_ψ/v_p are also plotted (dotted lines with circles). Resolution is 256 × 256 points.

In general, both v_ψ and v_ψ/v_p can change quite considerably both across the plasma in the same equilibrium and across different equilibria for the same machine. This is in part due to the variation of v_p across the cross section and in part to the fact that the difference between the magnetic and flux surfaces depends on the position in the plasma (see, e.g., Fig. 3). In conclusion, one should examine the equilibrium on a case by case basis to determine the importance of two-fluid equilibrium on stability properties.

As a final note it is known[37] that the effect of a normal component of the velocity on tearing stability vanishes if the electric potential Φ is $\Phi = \Phi(\psi, |B|)$. From Eq. (13), it is found that

$$\Phi = \frac{1}{e}\left[m_i\frac{v^2}{2} + \frac{\gamma_i}{\gamma_i - 1}S_i(\Psi)n^{\gamma_i - 1} - H_i(\Psi)\right] = \frac{1}{e}\left[H_e(\psi) - \frac{\gamma_e}{\gamma_e - 1}S_e(\psi)n^{\gamma_e - 1}\right]. \quad (57)$$

Looking at Eq. (21), there is no reason why n should be $n(\psi, |B|)$; the same functional dependence carries over to Φ. Thus, the effect of v_ψ on tearing stability does not automatically vanish, and it will need to be evaluated more in detail.

X. CONCLUSIONS AND FUTURE WORK

In this work, a new, versatile, and user-friendly two-fluid axisymmetric equilibrium code was introduced. It was proven that the two-fluid system with flow reduces to the MHD equilibrium with flow problem in the single-fluid limit with an approach different from the one in Ref. 10. It was also verified numerically that the single-fluid limit is recovered by FLOW2, which both confirms the theoretical result and improves our confidence in the code. The static limit was also recovered, but that was possible only by assigning the input free functions in the correct fashion.

One important element of this work is the formulation of the equilibrium problem in terms of "intuitive" free functions related to the ones in Ref. 5 with the purpose of making the use of the code as simple and intuitive as possible. In that spirit, the code is also made freely available for download in Ref. 38. In addition to the source files, the website also contains the input files for the equilibria presented in this work. One interesting element about the plasma rotation is that edge rotation cannot be assigned completely freely. As in single-fluid equilibrium, an excessive level of poloidal rotation will result in the Bernoulli equation not having any solution. In addition to this, toroidal rotation is proportional to the difference between the fluid and magnetic stream functions. Thus, its edge value must be assigned taking into account this fact. Under the same token, the boundary condition for the flow function Ψ must be assigned taking into account the edge value of the toroidal velocity. If this is ignored, convergence issues arise and it may become impossible to find an equilibrium solution.

Equilibria were calculated in several different conditions, both for spherical tokamak (NSTX) and standard tokamak (DIII-D) geometry. Equilibrium results were used to show that the static (two-fluid) and the MHD (single-fluid) limits are correctly recovered by the two-fluid model presented in this work. It was also shown that the "proper" plasma boundary is a "flow" rather than a "magnetic" surface, as in general there is finite equilibrium flow across any magnetic surface. It was suggested that this may have an effect on the stability of slow growing modes.

We close our discussion by observing that the development of FLOW2 opens several potential avenues of investigation, which will be considered in future work. In particular, the FLOW2 formulation and implementation can be further extended to include one or more additional species. This could be done to model a plasma with an energetic ion population, which would be introduced as an additional species with a separate set of free functions, with an approach similar to the one in Ref. 39. Another possible extension of this work is in the modeling of plasmas with distinct ion species, e.g., hydrogen and one or more heavier species such as oxygen. This is a case of interest for astrophysical plasmas, in particular for magnetosphere physics.

ACKNOWLEDGMENTS

This work was performed under DOE Grants No. DE-FG02-93ER54215 and DE-SC0014196. Our thanks go to E. Hameiri, A. Boozer, A. Bortolon, and J. Ramos for useful discussion. One of the authors (L.G.) also thanks the Princeton Plasma Physics Laboratory for the hospitality offered during the preparation of this work.

[1]E. Hameiri, Phys. Fluids **26**, 230 (1983).
[2]S. Semenzato, R. Gruber, and H. P. Zehrfeld, Comput. Phys. Rep. **1**, 389 (1984).
[3]R. Iacono, A. Bondeson, F. Troyon, and R. Gruber, Phys. Fluids B **2**, 1794 (1990).
[4]A. J. C. Beliën, M. A. Botchev, J. P. Goedbloed, B. van der Holst, and R. Keppens, J. Comput. Phys. **182**, 91 (2002).
[5]L. Guazzotto, R. Betti, J. Manickam, and S. Kaye, Phys. Plasmas **11**, 604 (2004).
[6]L. C. Steinhauer, Phys. Plasmas **6**, 2734 (1999).
[7]L. C. Steinhauer and A. Ishida, Phys. Plasmas **13**, 052513 (2006).
[8]J. P. Goedbloed, Phys. Plasmas **11**, L81 (2004).
[9]A. Thyagaraja and K. G. McClements, Phys. Plasmas **13**, 062502 (2006).
[10]E. Hameiri, Phys. Plasmas **20**, 092503 (2013).
[11]A. Ito, J. J. Ramos, and N. Nakajima, Plasma Fusion Res. **3**, 034 (2008).
[12]A. Ishida and L. C. Steinhauer, Phys. Plasmas **19**, 102512 (2012).
[13]E. Hameiri, Phys. Plasmas **20**, 022112 (2013).
[14]Y. Kawazura and E. Hameiri, Phys. Plasmas **19**, 082513 (2012).
[15]A. Ishida, L. C. Steinhauer, and Y.-K. M. Peng, Phys. Plasmas **17**, 122507 (2010).
[16]K. G. McClements and A. Thyagaraja, Mon. Not. R. Astron. Soc. **323**, 733 (2001).
[17]J. P. Goedbloed, Phys. Plasmas **12**, 064702 (2005).
[18]R. Betti and J. P. Freidberg, Phys. Plasmas **7**, 2439 (2000).
[19]J. L. Luxon and L. G. Davis, Fusion Technol. **8**, 441 (1985).
[20]J. L. Luxon, R. Anderson, R. Batty, C. B. Baxi, G. Bramson, N. H. Brooks, B. Brown, B. Burley, K. H. Burrell, R. Callis, G. Campbell, T. N. Carlstrom, A. P. Colleraine, J. Cummings, L. Davis, J. C. DeBoo, S. Ejima, R. Evanko, H. Fukumoto, R. Gallix, J. Gilleland, T. Glad, P. Gohil, A. Gootgeld, R. J. Groebner, S. Hanai, J. Haskovec, E. Heckman, M. Heiberger, F. J. Helton, N. Hosogane, C.-L. Hsieh, G. L. Jackson, G. Jahns, G. Janeschitz, E. Johnson, A. G. Kellman, J. S. Kim, J. Kohli, A. Langhorn, L. L. Lao, P. Lee, S. Lightner, J. Lohr, M. A. Mahdavi, M. Mayberry, B. McHarg, T. McKelvey, R. Miller, C. P. Moeller, D. Moore, A. Nerem, P. Noll, T. Ohkawa, N. Ohyabu, T. H. Osborne, D. O. Overskei, P. I. Petersen, T. W. Petrie, J. Phillips, R. Prater, J. Rawls, E. E. Reis, D. Remsen, P. Riedy, P. Roch, K. Schaubel, D. P. Schissel, J. T. Scoville, R. Seraydarian, M. Shimada, T. Shoji, B. Sleaford, Jr., J. P. Smith, P. Smith, T. Smith, R. T. Snider, R. D. Stambaugh, R. Stav, H. S.

John, R. E. Stockdale, E. J. Strait, R. Street, T. S. Taylor, J. Tooker, M. Tupper, S. K. Wong, and S. Yamaguch, *Plasma Physics and Controlled Fusion Research* (International Atomic Energy Agency, Vienna, 1987), Vol. I, p. 159.
[21]A. Ishida, C. O. Harahap, L. C. Steinhauer, and Y.-K. M. Peng, Phys. Plasmas **11**, 5297 (2004).
[22]A. Ito, J. J. Ramos, and N. Nakajima, Phys. Plasmas **14**, 062502 (2007).
[23]M. Ono, S. Kaye, Y.-K. Peng, G. Barnes, W. Blanchard, M. Carter, J. Chrzanowski, L. Dudek, R. Ewig, D. Gates, R. Hatcher, T. Jarboe, S. Jardin, D. Johnson, R. Kaita, M. Kalish, C. Kessel, H. Kugel, R. Maingi, R. Majeski, J. Manickam, B. McCormack, J. Menard, D. Mueller, B. Nelson, B. Nelson, C. Neumeyer, G. Oliaro, F. Paoletti, R. Parsells, E. Perry, N. Pomphrey, S. Ramakrishnan, R. Raman, G. Rewoldt, J. Robinson, A. Roquemore, P. Ryan, S. Sabbagh, D. Swain, E. Synakowski, M. Viola, M. Williams, J. Wilson, and NSTX Team, Nucl. Fusion **40**, 557 (2000).
[24]L. L. Lao, H. S. John, R. D. H. Stambaugh, A. G. Kellman, and W. Pfeiffer, Nucl. Fusion **25**, 1611 (1985).
[25]R. F. Schmitt, L. Guazzotto, H. Strauss, G. Y. Park, and C.-S. Chang, Phys. Plasmas **18**, 022502 (2011).
[26]T. K. M. Nakamura and M. Fujimoto, Geophys. Res. Lett. **32**, L21102, doi:10.1029/2005GL023362 (2005).
[27]T. K. M. Nakamura, M. Fujimoto, and A. Otto, J. Geophys. Res. **113**, A09204, doi:10.1029/2007JA012803 (2008).
[28]B. N. Rogers, R. E. Denton, and J. F. Drake, J. Geophys. Res. **108**, 1111, doi:10.1029/2002JA009699 (2003).
[29]L. Zakharov and B. Rogers, Phys. Fluids B **4**, 3285 (1992).
[30]D. Biskamp and T. Sato, Phys. Plasmas **4**, 1326 (1997).
[31]B. Rogers and L. Zakharov, Phys. Plasmas **3**, 2411 (1996).
[32]M. T. Beidler and P. A. Cassak, Phys. Rev. Lett. **107**, 255002 (2011).
[33]B. Rogers and L. Zakharov, Phys. Plasmas **2**, 3420 (1995).
[34]D. Biskamp, Phys. Plasmas **4**, 1964 (1997).
[35]D. P. Brennan and L. E. Sugiyama, Phys. Plasmas **13**, 052515 (2006).
[36]D. Brunetti, J. P. Graves, W. A. Cooper, and C. Wahlberg, Plasma Phys. Controlled Fusion **56**, 075025 (2014).
[37]A. H. Boozer, Phys. Plasmas **16**, 052505 (2009).
[38]See http://www.auburn.edu/cosam/faculty/physics/guazzotto/research/FLOW2_main.html for FLOW2 source files, sample inputs and outputs, including the inputs used for this paper.
[39]M. J. Hole and G. Dennis, Plasma Phys. Controlled Fusion **51**, 035014 (2009).